Multitarget nociceptor sensitization by a promiscuous peptide from the venom of the King Baboon spider

Rocio K. Finol-Urdaneta[a,b,c,1], Rebekah Ziegman[d], Zoltan Dekan[d], Jeffrey R. McArthur[a,c], Stewart Heitmann[e], Karen Luna-Ramirez[a,c], Han-Shen Tae[a,c], Alexander Mueller[d,2], Hana Starobova[d], Yanni K.-Y. Chin[d,f], Joshua S. Wingerd[d,3], Eivind A. B. Undheim[f,g,h], Ben Cristofori-Armstrong[d,i], Adam P. Hill[e,j], Volker Herzig[d,k], Glenn F. King[d,l], Irina Vetter[d,m], Lachlan D. Rash[d,i], David J. Adams[a,c,1], and Paul F. Alewood[d,1]

[a]Illawarra Health and Medical Research Institute, Wollongong, NSW 2522, Australia; [b]Electrophysiology Facility for Cell Phenotyping and Drug Discovery, Wollongong, NSW 2522, Australia; [c]Faculty of Science, Medicine and Health, University of Wollongong, Wollongong, NSW 2522, Australia; [d]Institute for Molecular Bioscience, University of Queensland, St. Lucia, QLD 4072, Australia; [e]Victor Chang Cardiac Research Institute, Darlinghurst, NSW 2010, Australia; [f]Centre for Advanced Imaging, University of Queensland, St. Lucia, QLD 4072, Australia; [g]Centre for Biodiversity Dynamics, Department of Biology, Norwegian University of Science and Technology, 7491 Trondheim, Norway; [h]Centre for Ecology and Evolutionary Synthesis, Department of Bioscience, University of Oslo, 0316 Oslo, Norway; [i]School of Biomedical Sciences, University of Queensland, St. Lucia, QLD 4072, Australia; [j]St Vincent's Clinical School, University of New South Wales Sydney, Darlinghurst, NSW 2010, Australia; [k]School of Science, Technology & Engineering and GeneCology Research Centre, University of the Sunshine Coast, Sippy Downs, QLD 4556, Australia; [l]Australian Research Council Centre of Excellence for Innovations in Peptide and Protein Science, University of Queensland, St. Lucia, QLD 4072, Australia; and [m]School of Pharmacy, University of Queensland, Woolloongabba, QLD 4102, Australia

Edited by Bruce Bean, Department of Neurobiology, Harvard Medical School, Boston, MA; received June 30, 2021; accepted November 23, 2021

The King Baboon spider, *Pelinobius muticus*, is a burrowing African tarantula. Its impressive size and appealing coloration are tempered by reports describing severe localized pain, swelling, itchiness, and muscle cramping after accidental envenomation. Hyperalgesia is the most prominent symptom after bites from *P. muticus*, but the molecular basis by which the venom induces pain is unknown. Proteotranscriptomic analysis of *P. muticus* venom uncovered a cysteine-rich peptide, δ/κ-theraphotoxin-Pm1a (δ/κ-TRTX-Pm1a), that elicited nocifensive behavior when injected into mice. In small dorsal root ganglion neurons, synthetic δ/κ-TRTX-Pm1a (sPm1a) induced hyperexcitability by enhancing tetrodotoxin-resistant sodium currents, impairing repolarization and lowering the threshold of action potential firing, consistent with the severe pain associated with envenomation. The molecular mechanism of nociceptor sensitization by sPm1a involves multimodal actions over several ion channel targets, including $Na_V1.8$, $K_V2.1$, and tetrodotoxin-sensitive Na_V channels. The promiscuous targeting of peptides like δ/κ-TRTX-Pm1a may be an evolutionary adaptation in pain-inducing defensive venoms.

hyperexcitability | $K_V2.1$ | $Na_V1.8$ | pain | target promiscuity

The King Baboon spider, *Pelinobius muticus* (formerly *Citharischius crawshayi*) (1, 2), is a large, fawn-colored tarantula found in Kenya and Tanzania that feeds on beetles, cockroaches, and other spiders, but will occasionally hunt vertebrates, such as mice, lizards, snakes, and birds. Larger species of Old World tarantulas like *P. muticus* spend most of their time in burrows and, unless provoked, pose no immediate risk to humans. Little is known about *P. muticus* envenomations, but like other tarantulas, they have evolved formidable chelicerae along with a venom that delivers mechanically and chemically painful bites to defend against perceived threats (3).

The triggering of unpleasant sensory experiences using pain-producing toxins would likely discourage most potential aggressors (4). Pain development and discomfort are universal features of spider envenomation (5). Spider venoms contain neurotoxins that produce paralysis and toxicity to humans through their ability to modulate ion channels and receptors. For example, mature male Australian funnel-web spiders use alogogenic δ-hexatoxin peptides in their venom to deter vertebrate predators after they leave their burrows in search of females (6).

The study of spider-venom toxin pharmacology has uncovered a vast collection of molecular tools for exploring pain physiology. Examples of such venom-derived peptides include Hm1a from the Togo starburst tarantula *Heteroscodra maculata*, which was used to show for the first time that the voltage-gated sodium (Na_V) channel, $Na_V1.1$, is involved in the transduction of mechanical pain (7), whereas Tsp1a from a Peruvian *Thrixopelma* tarantula was used to identify a key role for $Na_V1.7$ in the chronic visceral pain associated with irritable bowel syndrome (8).

Despite suggestive evidence that African tarantulas produce potent neurotoxic venoms, their effects and molecular composition have not been thoroughly explored (9). Understanding

Significance

Pain development and discomfort are universal features of spider envenomation, yet severe pain arising from bites by Old World spiders is poorly understood. Molecular analyses of the venom of the King Baboon spider revealed abundant expression of the inhibitory cystine knot peptide Pm1a. Synthetic Pm1a induces pain in mice while simultaneously enhancing proexcitatory sodium currents and decreasing inhibitory potassium currents. These concomitant effects promote hyperexcitability in pain-sensing neurons that can be reversed by pharmacological inhibition of voltage-gated sodium channels. The coordinated modulation of excitatory and inhibitory ion channels involved in pain propagation may represent an economical and effective defense strategy in pain-inducing defensive venoms.

Author contributions: R.K.F.-U. designed research; R.K.F.-U., R.Z., Z.D., J.R.M., S.H., K.L.-R., H.-S.T., A.M., H.S., Y.K.-Y.C., J.S.W., E.A.B.U., and B.C.-A. performed research; J.R.M., S.H., A.P.H., V.H., G.F.K., I.V., L.D.R., D.J.A., and P.F.A. contributed new reagents/analytic tools; R.K.F.-U., R.Z., Z.D., J.R.M., K.L.-R., H.-S.T., A.M., H.S., Y.K.-Y.C., J.S.W., E.A.B.U., and B.C.-A. analyzed data; R.K.F.-U. wrote the paper; and Z.D., J.R.M., S.H., H.-S.T., A.M., Y.K.-Y.C., E.A.B.U., B.C.-A., A.P.H., V.H., G.F.K., I.V., L.D.R., D.J.A., and P.F.A. edited the manuscript.

The authors declare no competing interest.

This article is a PNAS Direct Submission.

[1]To whom correspondence may be addressed. Email: rfinolu@uow.edu.au, djadams@uow.edu.au, or p.alewood@imb.uq.edu.au.

[2]Present address: Department of Molecular Biology, Princeton University, Princeton, NJ 08544.

[3]Present address: Channel Biologics Pty Ltd., Sydney, NSW 2139, Australia.

This article contains supporting information online at http://www.pnas.org/lookup/suppl/doi:10.1073/pnas.2110932119/-/DCSupplemental.

Published January 24, 2022.

the physiological process of pain generation by venom components is of considerable importance and could underpin effective treatments (9).

In the present study, we analyzed the venom proteome of *P. muticus* and identified an algogenic inhibitory cystine knot (ICK) peptide, δ/κ-theraphotoxin-Pm1a (Pm1a). We synthesized sPm1a, determined its three-dimensional (3D) structure, and evaluated its effects in vivo, ex vivo, and on heterologously expressed ion channel targets. We show that the spontaneous and ongoing pain from *P. muticus* envenomation originates from ectopic firing of peripheral nociceptors as a result of Pm1a's synergistic modulation of multiple voltage-gated ion channels.

Results

Identification and Synthesis of Pm1a. *P. muticus* venom and constituent peptide toxins have previously been shown to modulate the activity of voltage-gated ion channels (1, 2). A subsequent proteotranscriptomic analysis of *P. muticus* venom identified a peptide with a monoisotopic mass of 4524.5 Da, named δ/κ-theraphotoxin-Pm1a (δ/κ-TRTX-Pm1a). The transcript encoding δ/κ-TRTX-Pm1a (Fig. 1*A*) was the sixth most abundant contig in the venom-gland transcriptome, with 38,213 transcripts per million (Fig. 1*B*), consistent with its identification as a major venom component during venom fractionation (Fig. 1*C*). δ/κ-TRTX-Pm1a is encoded as an 85-residue prepropeptide comprised of a 19-residue signal peptide, followed by a 24-residue propeptide and the 42-residue mature δ/κ-TRTX-Pm1a toxin (Fig. 1*A*). The mature toxin contains six cysteine residues that form three disulfide bridges, with a theoretical molecular mass of 4524.89 Da (M^+H^+ = 4525.89) (Fig. 1*E*). δ/κ-TRTX-Pm1a is homologous to a family of tarantula-venom peptides bearing the highly conserved N-terminal "GVDK motif" (1).

To enable full structural and functional characterization, δ/κ-TRTX-Pm1a was synthesized in two fragments using Fmoc solid-phase peptide synthesis. Reduced, full-length toxin was generated by native chemical ligation (details in *SI Appendix*, *Materials and Methods* and Fig. S1). After folding and purification, the obtained synthetic product (hereafter sPm1a) was indistinguishable by HPLC and mass spectrometry from δ/κ-TRTX-Pm1a isolated from venom (Fig. 1*D*).

Three-Dimensional Structure of sPm1a. The 3D structure of sPm1a was determined using NMR spectroscopy. The final ensemble of 20 structures (Fig. 1*F*) revealed a highly flexible C-terminal region and a moderately dynamic β-hairpin loop, which together lead to a high overall backbone atom root-mean-square deviation (RMSD) of 0.78 ± 0.20 Å. The backbone RMSD is much lower (0.23 ± 0.03 Å) for the relatively rigid regions (residues 3 to 27 and 31 to 35), suggesting that the structure is well defined when the flexible regions are excluded. The ensemble of sPm1a structures is of high stereochemical quality as judged by a MolProbity score of 1.7 ± 0.1 (*SI Appendix*, Table S1).

The disulfide-bond connectivity of sPm1a was unequivocally determined from preliminary structure calculations performed without disulfide-bond restraints (10). The dipolar connectivities in the NOESY spectrum are consistent with the pattern Cys7–Cys21, Cys14–Cys26, and Cys20–Cys34 (red tubes in Fig. 1*F*). The three disulfide bonds form a cystine knot in which the Cys7–Cys21 and Cys14–Cys26 disulfides and the intervening section of the polypeptide chain form a closed loop that is pierced by the Cys20–Cys34 disulfide bond. Together with a canonical β-hairpin that is supported by two of the disulfide bonds, the overall structure of sPm1a conforms to the ICK motif commonly adopted by spider toxins known to modulate voltage-gated ion channels (11).

In contrast to the highly disordered C terminus (residues 36 to 42), the N terminus of sPm1a is relatively inflexible. A hydrogen bond is formed between the backbone amide of Val2 and the carbonyl oxygen of Cys20 (Fig. 1*F*), stabilizing the N-terminal tail in a position that is in close proximity to the core of the peptide. Hydrophobic patches are commonly found on the surface of gating-modifier peptides (GMPs) from tarantulas, such as SGTx1 and GxTx-1E, and they are proposed to interact with both the hydrophobic membrane lipids and the voltage-sensor domain on target ion channels (12, 13). Accordingly, sPm1a has most of its hydrophobic residues (Tyr9, Leu-10, Phe11, Leu24, Tyr33, and Trp36) on one face of the peptide, and they form a distinctive hydrophobic patch on the opposite side to the N terminus (Fig. 1 *G* and *H*).

sPm1a Elicits Nocifensive Behaviors in Mice. To determine whether sPm1a can recapitulate the pain experienced after a *P. muticus* bite, we delivered the synthetic peptide directly to primary afferent terminals in the hindpaw of adult mice in vivo and evaluated the resulting behavioral responses. Intraplantar injection of sPm1a resulted in immediate and dose-dependent emergence of spontaneous nocifensive behaviors, including paw licking and flinching (flinches per 15 min: Control [Ctr]: 0.7 ± 0.2; 0.06 nmol sPm1a = 27.8 ± 3.5, $P < 0.05$; 0.6 nmol sPm1a = 187.0 ± 16.5, $P < 0.0001$; $n = 4$ to 8 per condition) (Fig. 2*A*) that persisted for ∼15 min (*SI Appendix*, Fig. S2). These sPm1a-induced nocifensive behaviors included a considerable TTX-resistant component, with intraplantar administration of TTX partially reversing paw flinching (flinches per 15 min: 0.6 nmol sPm1a + 0.02 nmol TTX = 74.4 ± 5.4; $P < 0.001$) (Fig. 2*A* and *SI Appendix*, Fig. S2). Consistent with a major contribution of TTX-R channels to sPm1a-induced effects, coadministration of the selective $Na_V1.8$ inhibitor A803467 (14) significantly reversed spontaneous pain behaviors (flinches per 15 min: 0.6 nmol sPm1a + 0.2 nmol A803467 = 93.8 ± 8.8; $P < 0.001$) (Fig. 2*A* and *SI Appendix*, Fig. S2). Substantial changes in mechanical paw withdrawal threshold (PWT; Ctr: 3.7 ± 0.1 g; 0.06 nmol sPm1a = 1.3 ± 0.2 g; $n = 6$; $P < 0.001$) (Fig. 2*B*) and thermal thresholds (withdrawal temperature: Ctr: 49.8 ± 0.3 °C; 60 pmol sPm1a = 46.9 ± 0.4 °C; $n = 6$, $P < 0.001$) (Fig. 2*C*) were also observed following sPm1a injection (Fig. 2*C*), indicating mechanical and thermal hypersensitivity. Both Na_V channel blockers, TTX and A803467, partially and significantly reduced mechanical allodynia (paw withdrawal force: 600 pmol sPm1a = 1.0 ± 0.1 g; 600 pmol sPm1a + 20 pmol TTX = 2.4 ± 0.3 g; 600 pmol sPm1a + 200 pmol A803467 = 2.5 ± 0.2 g; $n = 5$ to 8; $P < 0.001$) (Fig. 2*B*), suggesting the TTX-R component is not limited to the spontaneous nocifensive behavior but also plays a role in mechanical allodynia induced by sPm1a.

sPm1a Induces Hyperexcitability in Small Dorsal Root Ganglion Neurons. Nociceptors are sensory neurons with crucial roles in the generation and conduction of pain signals and sensitization following injury or inflammation underlying hyperalgesia. The cell bodies of most sensory neurons reside in the dorsal root ganglion (DRG) in which nociceptors are typically recognized by their small cell size relative to other cell types (15). DRG neuron subtypes display different action potential (AP) waveforms and electrophysiological signatures that are common to major subclasses (16). For practical reasons, the overriding DRG neuron distinction used here was based on cell size estimated by membrane capacitance measurements, which is directly proportional to cell membrane area. Relatively broad APs with a "hump" in the falling phase made evident by two local minima in the AP first derivative (dV/dt) (see *Insets* in Fig. 2 *D* and *E*) are considered a distinctive feature of nociceptors. We performed whole-cell patch-clamp recordings from dissociated small DRG neurons (C ≤ 25 pF, equivalent to cell diameter ≤ 30 μm) from adult mice in the presence and absence of sPm1a. Sensitization,

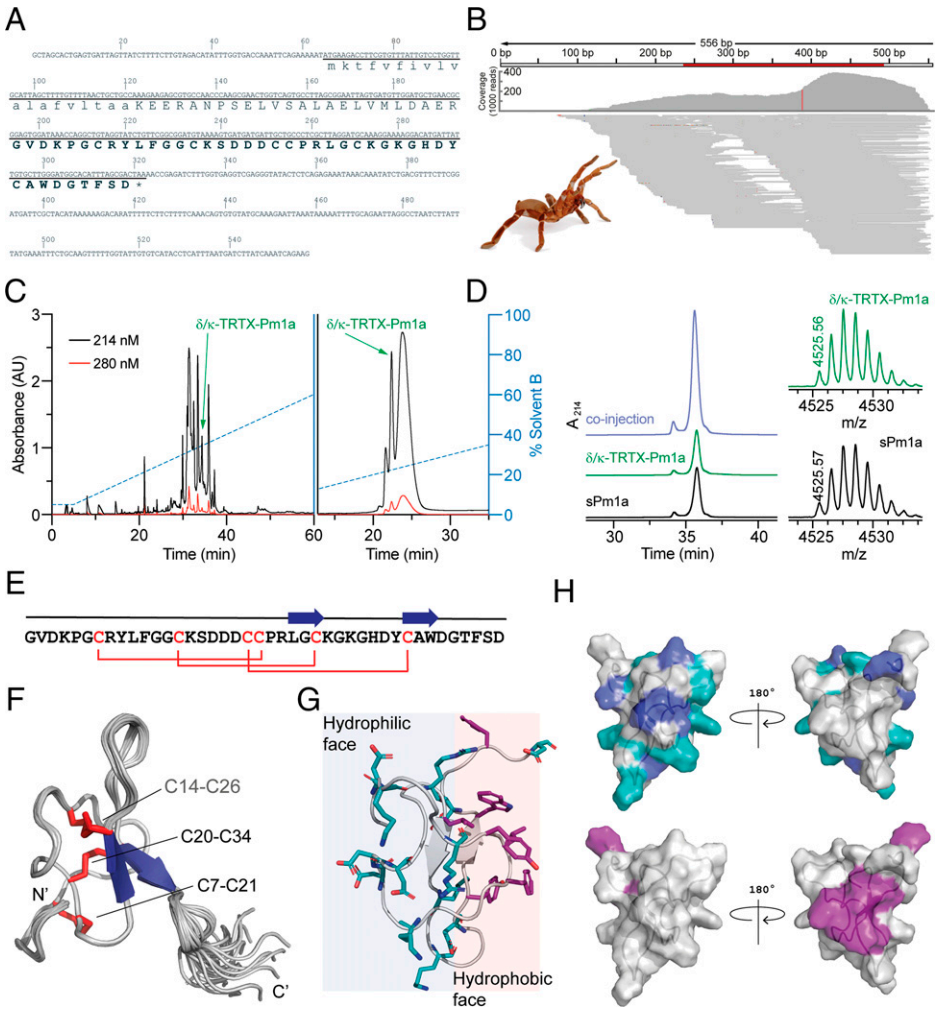

Fig. 1. Discovery and structural characterization of δ/κ-theraphotoxin-Pm1a. (*A*) *P. muticus* venom-gland transcript encoding δ/κ-TRTX-Pm1a with signal peptide in lowercase, propeptide in uppercase, and the mature peptide in bolded capitals. (*B*) Read coverage of the contig encoding δ/κ-TRTX-Pm1a, with an *Inset* showing King Baboon spider. Image credit: Shutterstock/Audrey Snider-Bell. (*C*) C_{18} RP-HPLC chromatogram showing fractionation of 0.5 mg crude *P. muticus* venom (*Left*) and purified δ/κ-TRTX-Pm1a (*Right*). (*D*) Chromatogram showing coelution of native δ/κ-TRTX-Pm1a and synthetic sPm1a. Absorbance was monitored at 214 nm. (*Right*) MALDI-TOF mass spectra, with the monoisotopic M^+H^+ shown for each peptide. (*E*) Mature peptide sequence highlighting disulfide connectivity and β-sheet regions. (*F*) Ensemble of sPm1a structures determined using NMR spectroscopy. Disulfide bonds are labeled and shown as red tubes while β-strands are shown in blue. (*G*) Structure of sPm1a showing hydrophilic and hydrophobic faces. (*H*) Surface representation showing distribution of sPm1a's hydrophilic residues (teal and cyan: *Upper*) and hydrophobic residues (purple: *Lower*).

manifested by increased neuroexcitability, is characteristic of nociceptors (17), whereas sPm1a exposure enhances the excitability of small DRG neurons. The current-clamp recording shown in Fig. 2*D* was obtained from a DRG neuron that fired spontaneously in control conditions (Fig. 2 *D*, *Upper*, black), while the addition of 1 μM sPm1a (Fig. 2 *D*, *Lower*, red) resulted in a two- to fourfold increase in firing frequency, AP peak amplitude, and AP half-width (quantification for this cell is in included in *SI Appendix*, Fig. S3). Note that the nociceptor AP hump evidenced by the first derivative of representative voltage responses (Fig. 2 *D*, *Inset*, dV/dt) in control conditions (Fig. 2*D*, black) displays the stereotypical two local minima that spread further apart in the presence of 1 μM sPm1a (Fig. 2*D*, red), suggestive of a repolarization delay in the presence of the venom peptide.

To compare excitability changes in small DRG neurons in the absence and presence of sPm1a, we used ramp current injections of 1 s duration (from 0 to 250 pA) (i.e., Fig. 2*E*, *Inset*), which allows simultaneous assessment of the number of APs and firing latency. The recordings shown in Fig. 2*E* display the firing responses of a 15 pF neuron stimulated by a subthreshold somatic ramp current injection (0 to 250 pA) in which exposure to sPm1a caused concentration-dependent increases in excitability. Under control conditions (Fig. 2*E*, black trace), no APs were observed, yet application of 0.1 μM sPm1a caused this cell to fire two APs (Fig. 2*E*, yellow), with progressively higher sPm1a concentrations increasing the number of APs fired (0.3 μM, Fig. 2*E*, green: 6 APs; 1 μM, Fig. 2*E*, red: 9 APs). Accordingly, the first AP fired appeared earlier (first latency) during the stimulation as the sPm1a concentration bathing this neuron was increased. Superimposed first derivative traces for the first AP fired in each condition are displayed in Fig. 2*E*, *Center Inset*, showing a concentration-dependent rightwards shift in the second local minima.

Sensitization of nociceptors develops as a consequence of tissue insult or inflammation and it is manifested as a reduction in the firing threshold or an increased response to noxious stimulation (17). Under control conditions, the firing characteristics of dissociated DRG neurons are notoriously heterogeneous. Paired responses in the absence (Ctr) and presence of 1 μM sPm1a from 36 small DRG neurons (obtained from seven independent isolations) are summarized in Fig. 2 *F*–*H*. First, we observed

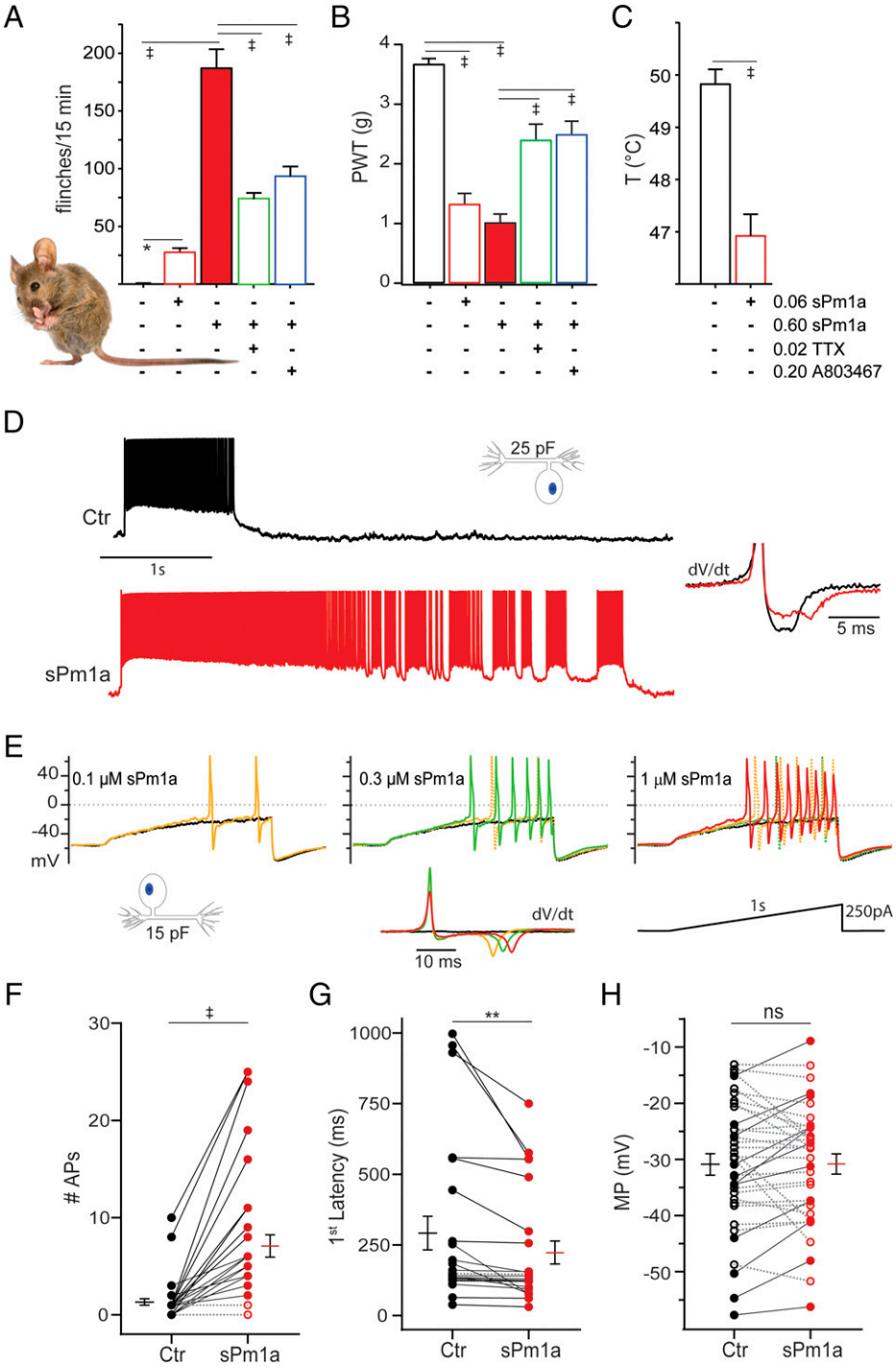

Fig. 2. sPm1a elicits nocifensive behavior in mice, induces hyperexcitability in small DRG neurons, and enhances the activity of TTX-R Na_V channels. sPm1a injection induces (*A*) dose-dependent spontaneous pain behavior (paw flinches/time), (*B*) mechanical allodynia (decreased PWT in g), and (*C*) thermal hypersensitivity (decreased paw withdrawal temperature thresholds) (doses are expressed in nmol/paw) (see *SI Appendix, Materials and Methods* for details). TTX and A803467 reverse spontaneous pain (*A*) and mechanical allodynia induced by sPm1a (*B*). (*B*) Image credit: Shutterstock/Eric Isselee. One-way ANOVA with Tukey's multiple comparison test: $^{*}P \leq 0.05$; $^{\ddagger}P \leq 0.0001$. (*D*) Spontaneous firing in a small DRG neuron (black, *Upper*) was enhanced by exposure to 1 µM sPm1a (red, *Lower*). The *Inset* shows the first derivative (dV/dt) of representative APs in the absence and presence of sPm1a (black and red, respectively). (*E*) sPm1a-evoked concentration-dependent increase in AP firing in a small DRG neuron. The ramp stimulation protocol (*Inset*, 1 s, 0 to 250 pA) applied in control conditions (black trace) did not elicit AP firing, whereas increasing concentrations of sPm1a caused a concentration-dependent increase in the number of APs fired upon the same stimulus (yellow: 0.1 µM; green: 0.3 µM; red: 1 µM sPm1a). The first derivative (dV/dt) of the first AP from the recordings on top is shown in the *Center Inset*. (*F–H*) Paired responses of mouse small DRG neurons before (Ctr) and after exposure to sPm1a (1 µM) and mean ± SEM (*F*) Individual and number of APs fired ($n = 36$), (*G*) first latency ($n = 24$; $^{**}P \leq 0.01$) and (*H*) membrane potential at the end of the ramp protocol (all neurons $n = 36$, $P = 0.9563$; responsive neurons $n = 11$, $P < 0.0001$). Solid symbols joined by solid lines and empty symbols joined by dotted lines correspond to sPm1a-responsive and nonresponsive DRG neurons, respectively. ns, not significant.

that sPm1a caused a significant increase in the number of APs fired (Fig. 2*F*) in 83% (30 of 36; number of APs_{Ctr} 1.3 ± 0.3 vs. number of APs_{sPm1a} 7.1 ± 1.2; $n = 36$, paired t test $P < 0.0001$). Second, sPm1a application significantly decreased the time to fire the first AP (Fig. 2*G*) in 89% (24 of 27) of the neurons in which a first latency could be measured in control conditions (during 1 s ramps) (Ctr: 257.1 ± 53.1 ms vs. sPm1a: 195.5 ± 34.8 ms; $n = 27$, paired t test $P = 0.0093$). Third, sPm1a had variable effects on the resting membrane potential, with depolarization observed in some neurons as well as either hyperpolarization or no change in others ($n = 36$, paired t test $P = 0.9563$) (Fig. 2*H*), likely reflecting the heterogeneity of the small DRG neurons tested.

From these observations, we infer that the function of δ/κ-TRTX-Pm1a within *P. muticus* venom involves sensitization of afferent neurons to maximize nociceptive signal generation upon the mechanical and chemical insults caused by bite puncture wounds and venom injection.

sPm1a-Enhanced Firing Involves Neuronal TTX-R Na_V and Delayed Rectifier K_V Conductances. AP firing in sensory neurons is largely determined by the voltage-gated sodium conductance carried by TTX-S and TTX-R Na_V channels. Small DRG neurons bathed in TTX at a concentration sufficient to completely block TTX-S Na_V channels were exposed to sPm1a. The firing responses of a small DRG neuron to ramp current injection (0 to 250 pA) bathed in TTX (0.5 μM) (Fig. 3 *A*, *Left*, dark gray), combined TTX and sPm1a (1 μM) (Fig. 3 *A*, *Center*, red) and after removal of sPm1a (Fig. 3 *A*, *Right*, light gray) are shown in Fig. 3*A*. The additive exposure of sPm1a (Fig. 3*A*, red) decreased latency to discharge, increased discharge activity, and impaired repolarization (right-shift in dV/dt local minima) (Fig. 3 *A*, *Inset* TTX: gray, sPm1a/TTX: red). Removal of sPm1a from the bath (washout: wo) immediately reversed DRG neuron firing behavior to that recorded prior to toxin exposure (Fig. 3*B*) ($n = 4$, ANOVA with Tukey's multiple comparisons test, TTX vs. TTX/sPm1a $P = 0.001$; TTX vs. wo $P > 0.9999$; TTX/sPm1a vs. wo $P = 0.0010$). As the contribution of TTX-S Na_V channels was pharmacologically abrogated in this small DRG neuron, the sensitizing effect of sPm1a on firing behavior appears to be supported by enhanced activity of TTX-R Na_V channels.

$Na_V1.8$ activity largely underlies DRG TTX-R Na^+ currents and these channels are abundantly expressed in nociceptive primary afferents where they are fundamental in mediating persistent pain (18, 19). The sPm1a-mediated increase in firing of DRG neurons was reversed by the $Na_V1.8$-blocker A803467, as shown in Fig. 3 *C* and *D*. Under control conditions, the cell shown fired six APs and adapted during the stimulation protocol (0 to 150 pA ramp). For this cell, sPm1a (0.3 μM) (Fig. 3*C*, green) significantly delayed adaptation resulting in an approximately threefold increase in the number of APs. The AP waveform exhibited a clear rising phase inflection in the first derivative (Fig. 3C, *Inset*) with a diverging pattern of activity for APs evoked in the presence of 0.3 μM sPm1a and those recorded in the absence of peptide (Fig. 3*C*, green and black dV/dt, respectively). Consistent with previous reports (14), the application of A803467 (1 μM) abolished sPm1a-induced neuronal firing (Fig. 3 *C* and *D*, blue) ($n = 6$, one-way ANOVA with Tukey's multiple comparisons test: Ctr vs. sPm1a $P = 0.005$; Ctr vs. A803467 $P = 0.5989$; sPm1a vs. A803467/sPm1a $P = 0.0007$), supporting the involvement of $Na_V1.8$ channels in the sensitizing effects of this spider-venom peptide. Although AP firing was abolished by inhibition of $Na_V1.8$, the membrane potential at the end of the stimulus ramp remained depolarized (red arrow in Fig. 3 *C*, *Right*) compared to control conditions (Fig. 2 *F–H*, cells represented as solid symbols joined by solid lines), suggesting additional effects of sPm1a over other small DRG neuron conductances.

When assessed under voltage clamp, whole-cell Na_V currents from small sensory neurons in the presence of TTX (0.5 μM) were augmented significantly by sPm1a as can be observed from the recordings shown in Fig. 3*E* (stimulus: 25 ms, −10 mV, Vh −80 mV, 0.1 Hz). The dark gray current traces in Fig. 3*E* correspond to the total TTX-R component of the DRG neuron Na^+ current. In the presence of TTX (0.5 μM), exposure to sPm1a (1 μM) resulted in a large increase in inward current (Fig. 3*E*, red) that was reversed by removing sPm1a from the bath containing TTX. This can be readily seen in the diary plot of the accumulated charge during the stimulus estimated by integrating the area under the current trace (Fig. 3 *E*, *Right*). In small DRG neurons, application of sPm1a (1 μM) (Fig. 3*E*, red) caused an average 6.1 ± 2.8-fold increase in charge mediated by TTX-R Na_V channels ($n = 6$). Removal of sPm1a from the bath solution allowed TTX-R Na^+ currents to return to control magnitude whereas application of A803467 (1 μM) reduced the sPm1a-sensitive TTX-R Na_V component of small mouse DRG neurons by 87.3 ± 11.1% ($n = 5$).

The suppression of sPm1a-enhanced firing and TTX-R Na^+ current reduction by the $Na_V1.8$-selective inhibitor A803467 suggests that the increase in AP firing is largely driven by enhancement of $Na_V1.8$-mediated Na^+ currents. However, TTX-R $Na_V1.9$ channels are also expressed in DRG neurons. The use of a pulse protocol favoring $Na_V1.9$ activation did not reveal a substantial contribution of this isoform in the population analyzed here (*SI Appendix*, Fig. S4), hampering our ability to assess the effects of sPm1a on $Na_V1.9$ mediated currents.

The first derivative of the voltage response to current injection in small DRGs exposed to sPm1a was typically right-shifted in the time axis indicating impairment in AP repolarization (*Insets* in Figs. 2 *D* and *E* and 3 *A* and *C*). Pharmacological inhibition of TTX-R currents suppressed AP firing but the membrane potential remained depolarized in about a third of the small DRG neurons recorded (Fig. 2*H*, solid circles joined by solid lines; i.e., arrow in Fig. 3*C*). Therefore, we assessed whether the K_V conductance of mouse small DRG neurons was modulated by sPm1a. Fig. 3*F* portrays a representative family of outward K^+ current traces obtained from a standard current–voltage (I-V) protocol in control (Fig. 3*F*, black, K_V total) and after the addition of 1 μM sPm1a, thereby observing a sPm1a-resistant K_V current (sPm1a-R) (Fig. 3*F*, gray dotted traces). Point-to-point subtraction revealed the sPm1a-sensitive (sPm1a-S) K_V component as a slow-activating outward current (Fig. 3*F*, red), with voltage dependence of activation ($V_{0.5}$: 5.8 ± 2.2 mV, $n = 9$) (*SI Appendix*, Fig. S5*A*) similar to that of recombinant $K_V2.1$ channels ($V_{0.5}$: 6.0 ± 0.8 mV, $n = 7$) (Fig. 4). We also used a double-pulse protocol in which 5-s duration depolarizing prepulses (from −90 to +40 mV) maximally inactivated A-type small DRG K_V channels to better observe the delayed rectifier (KDR) component of neuronal K_V (*SI Appendix*, Fig. S5*B*). Application of sPm1a (1 μM) under these conditions caused a significant 30 to 40% reduction of KDR at all prepulse potentials tested ($n = 5$; Ctr vs. sPm1a at each prepulse potential paired t test $P < 0.05$) (Fig. 3*F* and *SI Appendix*, Fig. S5).

sPm1a Enhances $Na_V1.8$ and Inhibits $K_V2.1$ Channels. In nociceptors, $Na_V1.8$ and the KDR are the dominating conductances of the AP (20). $K_V2.1$ homo- and heteromeric channels mediate the majority of the delayed rectifier K_V current in small DRG neurons (21), and because of their slow activation and inactivation kinetics the activity of K_V2 channels is expected to contribute significantly to neuronal repolarization/after-hyperpolarization (22). We performed double immunostaining for $Na_V1.8$ and $K_V2.1$ channels in our primary cultures of dissociated small DRG neurons from adult mice. Fig. 4*A* shows confocal images of adult mouse DRG neurons in which $Na_V1.8$ (Fig. 4*A*, red) and $K_V2.1$ (Fig. 4*A*, green) are abundant and recognized within the same neurons as

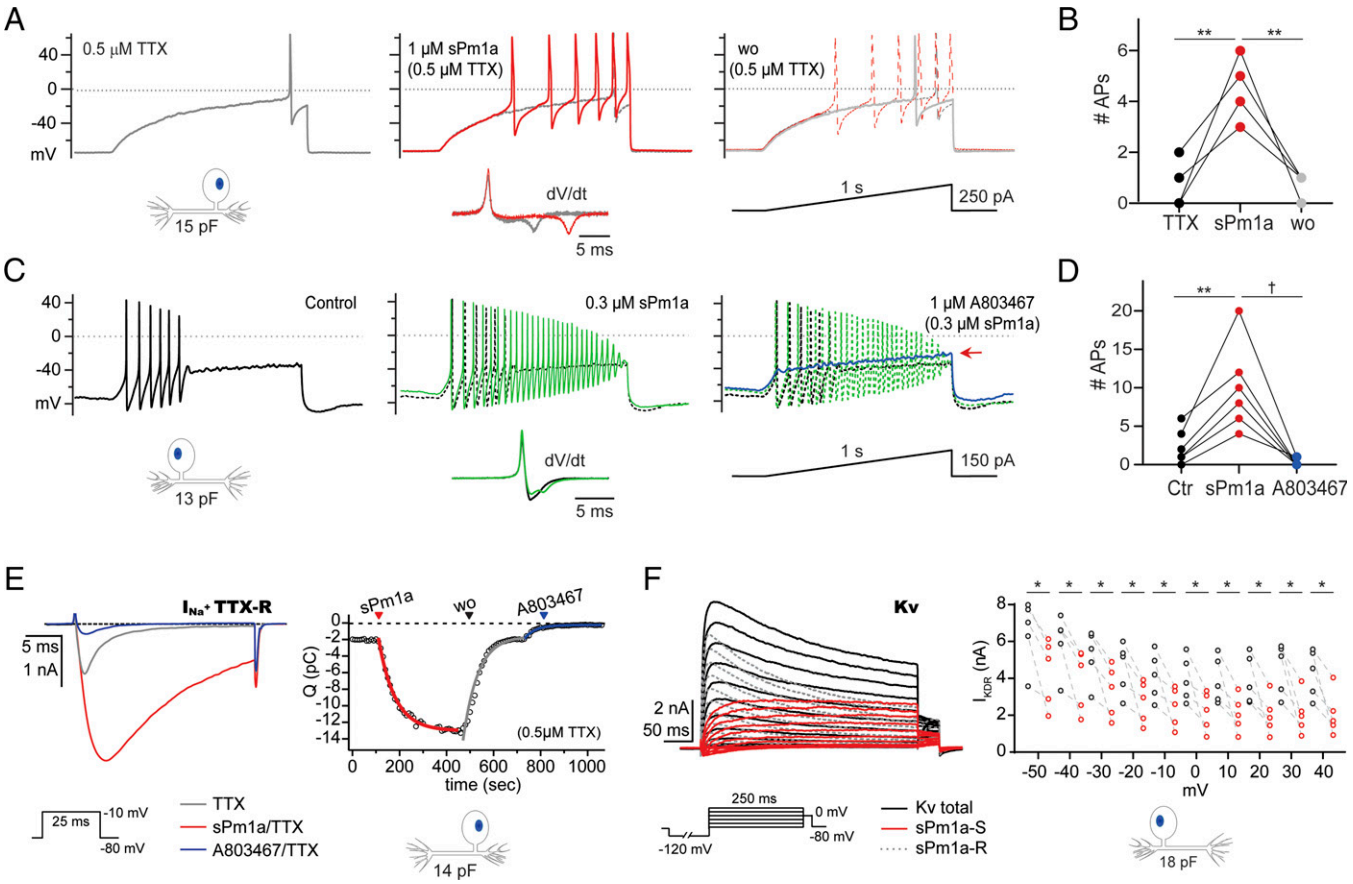

Fig. 3. sPm1a-enhanced firing is reversible and involves neuronal TTX-R Na_V and delayed rectifier K_V conductances. (*A*) Current-clamp recordings of a small DRG neuron stimulated with a ramp current injection (*Right Inset*) in the presence of TTX (0.5 μM; *Left*, dark gray), in a combination of TTX and sPm1a (1 μM; *Center*, red) and after washout of sPm1a (wo, *Right*, light gray). *Center Inset*: dV/dt of first AP before (dark gray) and after exposure to sPm1a (red, respectively). (*B*) Paired number of APs from neurons in (black circle: TTX), in sPm1a (red circle: TTX/sPm1a), and after washout (gray circle: wo). One-way ANOVA with Tukey's multiple comparisons test: $^{**}P \leq 0.01$. (*C*) Firing responses of an adapting small DRG neuron. Control (*Left*, black); exposure to sPm1a (0.3 μM; *Center*, green) and complete inhibition of firing upon exposure to A803467 (1 μM; *Right*, blue). Depolarized membrane potential at the end of the ramp in the A803467-inhibited condition is marked by the red arrow. *Center Inset*: dV/dt plot of first AP in absence and presence sPm1a (black and green, respectively). *Right Inset*: stimulation protocol. (*D*) Paired number of APs from neurons in control (black circle), in sPm1a (1 μM, red circle), and after addition of A803467 (1 μM, blue circle). One-way ANOVA with Tukey's multiple comparisons test: $^{**}P \leq 0.01$; $^{\dagger}P \leq 0.001$. (*E*) (*Left*) Voltage-clamp recording of small DRG neuron TTX-R Na^+ current elicited by a depolarizing pulse (*Inset*, 25 ms, −10 mV, Vh −80 mV) in the presence of TTX (0.5 μM, dark gray). Exposure to sPm1a (1 μM, red) and A803467 (1 μM, blue). (*Right*) Diary plot showing reversible TTX-R enhancement by sPm1a and complete inhibition of the sPm1a-sensitive TTX-R component by A803467. (*F*, *Left*) DRG K_V currents in the absence (black, K_V total) and presence of 1 μM sPm1a (gray dotted, sPm1a-R). sPm1a sensitive K_V currents are evidenced by point-to-point subtraction (red, sPm1a-S). (*Right*) Small DRG neuron I_{KDR} measured after 5-s prepulses to progressively depolarized potentials (*SI Appendix*, Fig. S5*B*) in the absence and presence of 1 μM sPm1a ($n = 5$; paired *t* test for control vs. sPm1a at each prepulse potential, $^{*}P < 0.05$).

evidenced by overlap of individual fluorescence signals (Fig. 4 *A*, *Far Right*, and *SI Appendix*, Fig. S6).

sPm1a action on human $Na_V1.8$-mediated Na^+ currents in HEK293 cells mirrored its effect on mouse small DRG neurons (Fig. 3*E*), with $Na_V1.8$ currents enhanced by sPm1a in a concentration-dependent manner (Fig. 4*B*). Peak current amplitude, like other macroscopic current metrics, is a complex variable reflecting net changes in gating and conductance, therefore we tracked concentration-dependent effects of sPm1a by measuring the absolute charge (area under the curve) flowing during the stimulation pulse (25 ms, –10 mV, Vh –80 mV) at different concentrations of sPm1a. The concentration–response relationship shown in Fig. 4*C* was normalized to the absolute charge increase registered upon exposure to 10 μM sPm1a, giving an estimated EC_{50} of 1.1 ± 0.1 μM ($n_H = 1.5 \pm 0.1$, $n = 3$ to 9 per concentration) for enhancement of $hNa_V1.8$ currents.

The primary and tertiary structure of sPm1a resembles those of venom-derived GMPs. In order to evaluate the effect of sPm1a on recombinant $Na_V1.8$ channels, we compared Na^+ currents in the absence and presence of 1 μM sPm1a (Fig. 4*D*, black and red, respectively) that were elicited by 100 ms depolarizing pulses from –80 mV to 50 mV, in 5-mV steps, from a holding potential of –80 mV. (Fig. 4 *D*, *Inset*). Comparison of Na^+ current families (shown in 10-mV steps for clarity) in control (Fig. 4*D*, black) and in the presence of sPm1a (Fig. 4*D*, red) revealed that the gating of $Na_V1.8$ is modified by this spider-venom peptide. sPm1a exposure caused a right-shift in $Na_V1.8$ steady-state inactivation (SSI, $V_{0.5}$: −38.7 ± 1.3 mV, $n = 8$; vs. −29.9 ± 1.3 mV, $n = 8$; $P = 0.0003$) (Fig. 4*E*, closed symbols) and delayed open-state inactivation kinetics (τ_{inact} at –10 mV: Ctr: 7.0 ± 1.0 ms, $n = 8$; sPm1a: 26.2 ± 3.6 ms, $n = 8$; $P = 0.0002$), resulting in a 16.7 ± 5.4% ($n = 16$) increase in the persistent currents recorded at the end of a 100 ms pulse to −10 mV (Fig. 4 *D* and *E*). An ∼8 mV hyperpolarizing shift in the voltage dependence of activation ($V_{0.5}$: −6.2 ± 1.1 mV, $n = 7$; vs. −14.5 ± 0.8 mV, $n = 16$; $P < 0.0001$) (Fig. 4*E*, open symbols) and a delay in activation kinetics (τ_{act} at –10 mV: Ctr: 0.5 ± 0.3 ms, $n = 5$; sPm1a: 1.6 ± 0.1 ms, $n = 5$; $P = 0.0083$) were detected in

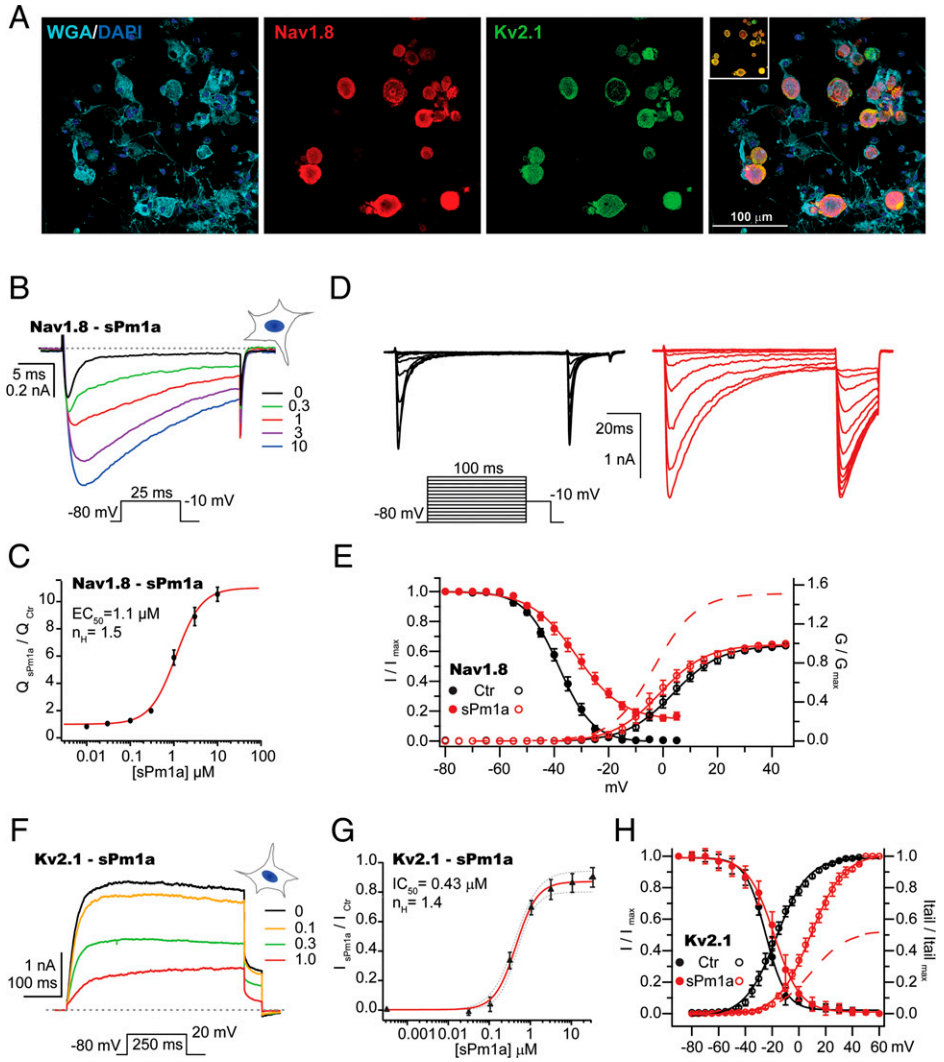

Fig. 4. sPm1a modulates recombinant $Na_V1.8$ and $K_V2.1$ channels. (*A*) Confocal images of adult mouse DRG neurons showing the overlap between fluorescent signals from $Na_V1.8$ (red) and $K_V2.1$ (green) epitopes (*Inset* on far-right panel). Counterstain is DAPI (blue) and WGA (cyan). (*B*) Recombinant $Na_V1.8$ whole-cell currents recorded in HEK293 cells activated by 25-ms pulses to –10 mV (Vh −80 mV, *Inset*) exposed to progressively higher concentrations of sPm1a (in µM) are shown in different colors. (*C*) Concentration–response relationship (CRC; EC_{50} = 1.1 ± 0.1 µM; n_H = 1.5 ± 0.1, n = 3 to 9 per point). (*D*) Families of $Na_V1.8$ currents in the absence (black) and presence of sPm1a (1 µM, red). (*Inset*) Stimulation protocol (100 ms, –80 mV to 50 mV, Δ5 mV and Vh –80 mV). Traces are shown every 10 mV for clarity. (*E*) Voltage-dependent activation and SSI of $Na_V1.8$. Normalized macroscopic conductance (G/G_{max}) in the absence (black open circle, $V_{0.5}$: −6.2 ± 1.1 mV, n = 7) and presence of sPm1a (1 µM, red open circle, $V_{0.5}$: −14.5 ± 0.8 mV, n = 16; unpaired t test $P < 0.0001$) calculated from peak currents from the protocol in *D*. The dashed trace corresponds to G_{sPm1a}/G_{Ctr} to highlight the effect of sPm1a on the macroscopic conductance of $Na_V1.8$. The voltage dependence of SSI was estimated from a double-pulse protocol (500-ms prepulse from −80 to 10 mV, Δ5 mV, 25 ms pulse to −10 mV, Vh −80 mV). Control (black circle, SSI $V_{0.5}$: −38.7 ± 1.3 mV, n = 8) and sPm1a (red circle, −29.9 ± 1.3 mV, n = 8; unpaired t test P = 0.0003). (*F*) Whole-cell $K_V2.1$ currents expressed in TSA201 cells activated by 250 ms pulses to 20 mV (Vh −80 mV, *Inset*) exposed to progressively higher concentrations of sPm1a (in µM) are shown in different colors. (*G*) Concentration–response curve for inhibition of recombinant $K_V2.1$ by sPm1a (IC_{50} = 0.40 ± 0.01 µM; n_H = 1.4, n = 7 per point). (*H*) $K_V2.1$ activation and SSI. Normalized $K_V2.1$ tail current ($Itail/Itail_{max}$) in the absence (black open circle, $V_{0.5}$: 6.05 ± 0.8 mV, n = 7) and presence of sPm1a (red open circle, $V_{0.5}$: 32.9 ± 0.4 mV, n = 7; unpaired t test P = 0.0001). The dashed trace corresponds to $Itail_{sPm1a}/Itail_{Ctr}$. Voltage dependence of $K_V2.1$ SSI was estimated from a double-pulse protocol (5-s prepulse from −90 to 60 mV, Δ10 mV, 250 ms pulse to 60 mV, Vh −80 mV) (*SI Appendix*, Fig. S5). Control (black circle, SSI $V_{0.5}$: −24.6 ± 3.5 mV, n = 5) and sPm1a (1 µM; red circle, −18.2 ± 4.9 mV, n = 5; unpaired t test P = 0.3189).

the presence of sPm1a. Hence, our data provide compelling evidence that sPm1a is a gating-modifier peptide that strongly potentiates rodent and human $Na_V1.8$-mediated currents.

The similarities in current kinetics, voltage dependence of activation, strong $K_V2.1$ immunoreactivity in mouse DRG neuron primary cultures and its frequent targeting by spider Na_V GMPs (23), prompted us to investigate the effects of sPm1a on human $K_V2.1$ heterologously expressed in mammalian cells using automated patch-clamp electrophysiology. We found $K_V2.1$ channels to be sensitive to sPm1a (Fig. 4*F*), with an IC_{50} of 0.4 ± 0.01 µM (n_H = 1.4, n = 7) (Fig. 4*G*). Similar to other spider-venom peptides like hanatoxin, sPm1a caused a ∼27-mV depolarizing shift in the voltage dependence of $K_V2.1$ activation ($V_{0.5}$: 32.9 ± 0.4 mV, n = 7; P = 0.0001) without significant changes in SSI (Ctr $V_{0.5}$: −24.6 ± 3.5 mV, n = 5, vs. sPm1a $V_{0.5}$: −18.2 ± 4.9 mV, n = 5; unpaired t test P = 0.3189) (Fig. 4*H*). Functional enhancement of repolarizing K_V currents depresses neuronal excitability in primary sensory neurons; thus, inhibition of KDR by a large shift in the activation voltage as verified for $K_V2.1$ channels suggests that sPm1a may also enhance excitability

by altering the neuronal refractory period. These results are consistent with a role for sPm1a inhibition of KDR currents in neuronal sensitization and hyperexcitability leading to pain perception upon *P. muticus* envenomation.

sPm1a Modulates Na_V Channels, But Not Nicotinic Acetylcholine Receptors. Gating-modifier spider-venom peptides often target multiple Na_V channels. Automated patch-clamp screening of human $Na_V1.1$–$Na_V1.7$ isoforms revealed that sPm1a nonselectively inhibits peak currents mediated by all these channels with IC_{50} values of 0.38 to 2.3 μM (*SI Appendix*, Table S2). In the presence of 1 μM sPm1a, depolarization-triggered fast inactivation was substantially delayed three- to fourfold for currents elicited by the TTX-S channels $Na_V1.1$, $Na_V1.3$, $Na_V1.6$, and $Na_V1.7$ (τ_{sPm1a}/τ_{Ctr} = 3.5 to 4.5) (*SI Appendix*, Table S3), which are abundantly expressed in peripheral neurons. In contrast, the inactivation kinetics of $Na_V1.2$ (brain), $Na_V1.4$ (skeletal muscle), and $Na_V1.5$ (cardiac muscle) were not significantly modified (τ_{sPm1a}/τ_{Ctr} ~1) (*SI Appendix*, Table S3).

Subexcitability is commonly attributed to inactivation of Na_V channels, and in small DRG neurons the TTX-S channel $Na_V1.7$ is important in setting the threshold of AP firing, ultimately regulating neuronal excitability (24–26). A closer examination of $Na_V1.7$ modification by sPm1a (1 μM) by manual patch-clamp of HEK293 cells revealed that this peptide slows $Na_V1.7$ fast inactivation by approximately threefold (τ_{inact} Ctr: 0.8 ± 0.2 ms, n = 6; vs. sPm1a: 2.7 ± 0.4 ms, n = 6; unpaired t test P = 0.0017) and shifts the voltage dependence of activation to more positive potentials ($V_{0.5}$ Ctr: −25.4 ± 1.8 mV, n = 5; vs. sPm1a: −10.6 ± 1.7 mV, n = 6; P = 0.0002) without evident changes to SSI (SSI $V_{0.5}$ Ctr: −75.5 ± 0.5 mV, n = 5; vs. sPm1a: −76.5 ± 0.4 mV, n = 7; P = 0.1458) (*SI Appendix*, Fig. S7).

We also examined whether the symptoms induced by *P. muticus* bites may be due in part to modulation of the nicotinic acetylcholine receptors (nAChRs) at the neuromuscular junction. We used two-electrode voltage-clamp electrophysiology to examine the effect of sPm1a on human (h) neuronal and rodent (r) muscle nAChR subtypes expressed in *Xenopus laevis* oocytes. The amplitude of acetylcholine-evoked currents mediated by hα3β2, hα4β2, hα7, rα1β1δγ, and rα1β1δε nAChRs were unchanged in the presence of 1 μM sPm1a (*SI Appendix*, Table S4), suggesting that cholinergic neurotransmission is not directly affected by sPm1a.

sPm1a modulation of TTX-S Na_V channels in nociceptive neurons, such as $Na_V1.7$, may contribute to the pain-sensitization evoked by sPm1a. However, the multimodal effects of sPm1a and compositional variability and amplitude of the TTX-S component in DRG neurons challenge our ability to rigorously elucidate the contribution of this conductance to modified excitability within the scope of this study. We have therefore attempted to address this question from a theoretical standpoint in the following section.

Modeling sPm1a-Induced Hyperexcitability of Small DRG Neurons. sPm1a modulates TTX-R $Na_V1.8$, delayed rectifier K_V currents, and TTX-S Na_V channels in small DRG neurons and their recombinant molecular counterparts in heterologous expression systems. The overall effects of sPm1a on a variety of small DRG neurons are consistent with sensitization through facilitation of repetitive firing, lower AP thresholds, and decreased firing latency. We, therefore, employed a mathematical model of nociceptor excitability to "dissect" the contribution of selected sPm1a-sensitive conductances in isolation and their concerted actions.

Hodgin–Huxley formulations of $Na_V1.8$ and TTX-S Na_V channels, based on those published by Verma et al. (27), were implemented in the Brain-Dynamics Toolbox (28) and $Na_V1.8$ currents were simulated in response to standard voltage-clamp protocols. Model parameters describing voltage dependence and rates of channel activation and inactivation (details in *SI Appendix*, Tables S5 and S6) (29) were adjusted to recapitulate $Na_V1.8$ behavior both at baseline and in the presence of sPm1a (Fig. 5*A*). This model of the $Na_V1.8$/sPm1a molecular interaction was then incorporated into a single-compartment model of small DRG neuron soma (26) to predict emergent effects on neuronal electrophysiology. In addition to modification of $Na_V1.8$ by sPm1a, the effects on KDR were modeled as a 30% decrease in conductance without changes to kinetic parameters as indicated by our experimental data (Fig. 3*D*). The TTX-S Na_V voltage dependence and rates parameters of activation and inactivation in control and in the presence of sPm1a are provided in *SI Appendix*, Table S7. Simulated effects on neuronal excitability of individual molecular targets of sPm1a ($Na_V1.8$/TTX-S/KDR) are presented in Fig. 5 and *SI Appendix*, Fig. S8. Under control conditions, current injection generates a single AP (Fig. 5 *B*, *Top*), consistent with our data from mouse DRG neurons. Inclusion of sPm1a-modified $Na_V1.8$ (in the absence of any sPm1a-dependent changes in KDR or TTX-S) increased the number of APs fired in the modeled neuron (Fig. 5*B*, red dotted trace, 2 APs), while inclusion of either reduced KDR conductance or altered TTX-S Na_V gating/conductance alone did not cause an increase in firing (Fig. 5 *B*, *Bottom*; dotted orange and blue traces, respectively, and Fig. 5 *D*, *Left*) and likely counteract each other (Fig. 5 *D*, *Center*, first latency for KDR and TTX-S). However, inclusion of the effects of all sPm1a targets ($Na_V1.8$, KDR, TTX-S) in the simulated neuron resulted in substantially enhanced excitability (Fig. 5 *C* and *D*), consistent with a typical mouse DRG neuron stimulated with an equivalent current injection (Fig. 5*E*), while the simulated number of APs and latency (Fig. 5 *D* and *E*) qualitatively reproduced our in vitro data (Fig. 2 *F* and *G*). Thus, the modifications that we implemented to the Mandge and Manchanda model (30) closely reflect the effects of sPm1a on small DRG neurons reported here.

A key motivation for computationally modeling biological observations is that it allows the study of variables in isolation that would otherwise not be possible, as it is the case of promiscuous ($Na_V1.8$, KDR, Na_V TTX-S, and so forth) and multimodally (gating and kinetics) active peptides like sPm1a. Of particular interest is how modification of TTX-Na_V conductance (TTX-S^C) and kinetics (TTX-S^K) contribute to the effects of sPm1a on neuronal excitability. Modeled traces resulting from independent incorporation of changes to TTX-S^C and TTX-S^K into $Na_V1.8$+KDR models (*SI Appendix*, Fig. S8) show that neither of these parameters in isolation (or combined) affects firing responses at the beginning of the current stimulus (*SI Appendix*, Fig. S8*C*). For the neuron in our reductionist model, inhibition of the TTX-S conductance progressively decreases the time between AP bursts which, in combination with an enhancement of $Na_V1.8$ and impairment of KDR, decreases the time between burst for later time points (*SI Appendix*, Fig. S8*E*). Notwithstanding, our model suggests that a sPm1a-like delay in TTX-S Na_V inactivation kinetics (TTX-S^K) appears to dominate over its inhibitory effects on this conductance (*SI Appendix*, Fig. S8 *C–E*).

It has been shown that TTX-S $Na_V1.7$ activation amplifies small depolarizations that bring peripheral neurons within firing threshold, with the $Na_V1.8$ conductance contributing the bulk of the inward current underlying the AP upstroke during repetitive firing of pain-sensing neurons (31). Experimentally, sPm1a inhibits peak currents and delays fast inactivation of TTX-S Na_V channels (*SI Appendix*, Fig. S7 and Tables S2 and S3). Overall, our computational approach lends support to the notion that modification of the $Na_V1.8$ current alone increases neuronal excitability, yet it is insufficient to fully recapitulate our experimental observations and therefore the additional inhibition of KDR is required for the enhancement of excitability observed in small DRG neurons. Furthermore, multimodal modification of TTX-S Na_V channels may also contribute to sPm1a's actions depending on the complement and relative contribution of TTX-S Na_V channels present in individual DRG neurons.

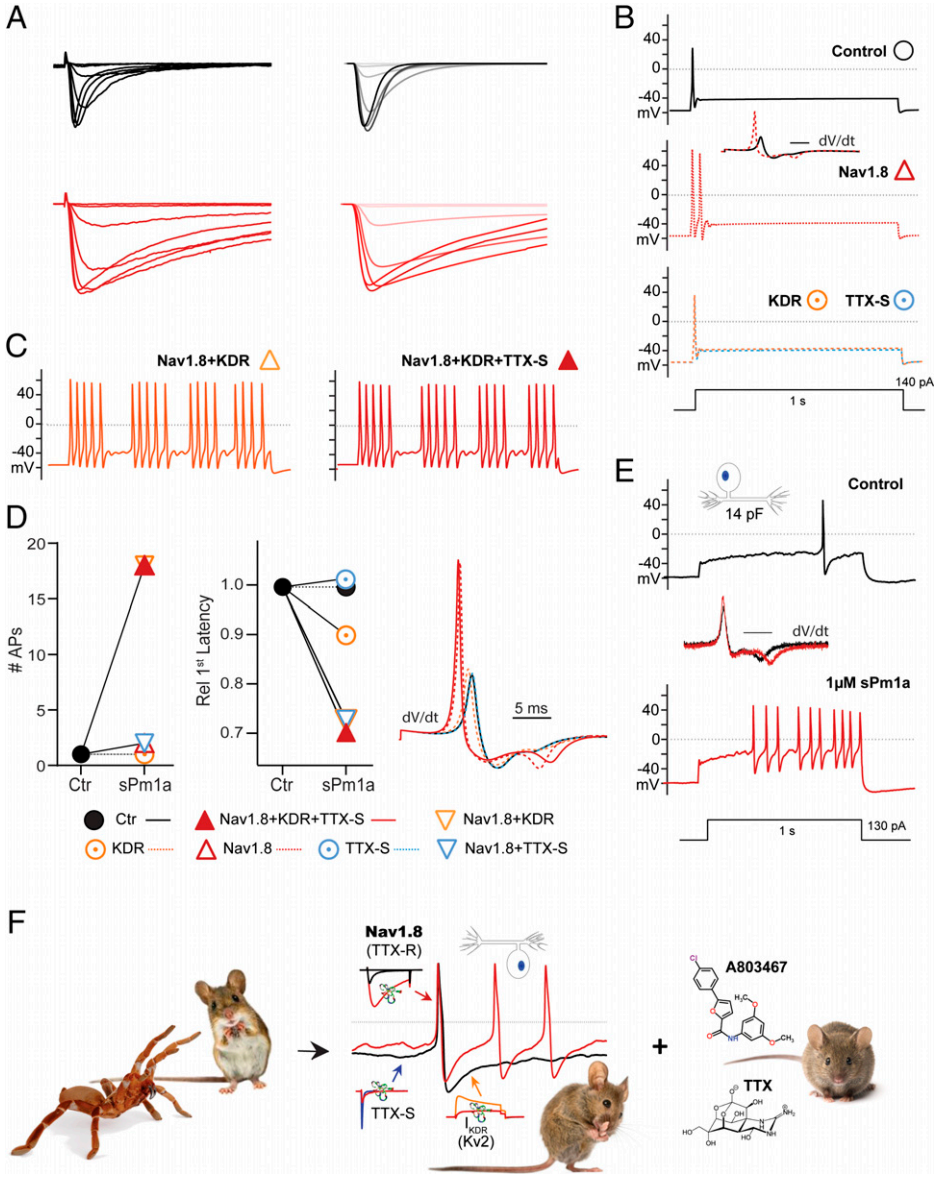

Fig. 5. Compounded effects of sPm1a on small DRG Na_V and K_V conductances contribute to neuronal sensitization. Modeling of sPm1a-induced changes in $Na_V1.8$, KDR, and TTX-S Na_V nociceptor excitability. (*A*) Experimentally recorded $Na_V1.8$-mediated currents (*Left*) in the absence (black) and presence of sPm1a (1 μM) and corresponding Hodgkin and Huxley formalism fitted traces (*Right*). (*B–D*) The model nociceptor was stimulated with a 1 s step current injection of 140 pA (*Bottom Inset* in *B*). (*B*, *Top*) Model nociceptor firing under control conditions (black). (*Middle*) Trace resulting from implementation of sPm1a-modified $Na_V1.8$ parameters from *A* (*SI Appendix*, Table S5) showing an increase in number of APs (red) and a shift in the second local minima in dV/dt (*Inset*). (Scale bar, 5 ms.) (*Bottom*) Traces from individually modeled sPm1a-like inhibition of KDR (orange dotted) and modification of TTX-S conductance (blue dotted). (*C*) Model nociceptor responses compounding sPm1a effects on $Na_V1.8$ and KDR (*Left*, orange) or modification of $Na_V1.8$, KDR, and TTX-S (*Right*, red). (*D*) Quantification of number of APs, relative first latency (first lat_X/first lat_{Ctr}), and expanded first derivative dV/dt of the first AP number of modeled data from each condition. Legend is shown below. (*E*) Recorded membrane potential responses from a mouse small DRG neuron to a step stimulus (*Bottom Inset*) in the absence (*Top*, black) and presence of sPm1a (1 μM, red, *Bottom*). The first derivative analysis traces to the first AP in both conditions is shown in the *Inset*. (Scale bar, 5 ms.) (*F*) Proposed mechanism of sPm1a-induced nociceptor sensitization and its pharmacological reversal. Pm1a produces nociceptor sensitization by promoting repetitive firing (enhancement of $Na_V1.8$ currents) and impairing repolarization (inhibition of delayed rectifier K_V channels) with a potential contribution from the modulation of TTX-S Na_V channels. Pm1a-induced hyperexcitability can be reversed by inhibition of $Na_V1.8$ and TTX-S Na_V currents. From left to right, image credits: Shutterstock/Audrey Snider-Bell; Shutterstock/Rudmer Zwerver; Shutterstock/Eric Isselee; Shutterstock/Egoreichenkov Evgenii.

Discussion

Spontaneous activity and increased firing frequency of nociceptors are the key sources of pain in the peripheral nervous system. Although many venom-derived peptides promiscuously modulate the activity of ion channels involved in nociception, their combined actions on neuronal excitability have not been thoroughly elucidated (32). In this study, we identified a peptide from *P. muticus* venom, δ/κ-TRTX-Pm1a, chemically synthesized sPm1a, determined its 3D structure, and functionally characterized its actions, in vivo, ex vivo, and heterologous expression systems. Mathematical modeling supported our functional findings whereby sPm1a enhances nociceptor excitability mainly by the simultaneous stimulation of repetitive firing (through TTX-R $Na_V1.8$ current enhancement) and impairment of repolarization (by inhibiting KDR, $K_V2.1$), with a potential contribution from TTX-S Na_V modified excitability, leading to manifestations of

pain behavior in mice and their reversal through inhibition of $Na_V1.8$ and TTX-S Na_V channels (Fig. 5*F*).

sPm1a modulates the availability of the quintessentially nociceptive channels $Na_V1.8$ and $Na_V1.7$, as well as a major contributor to membrane repolarization, $K_V2.1$, to produce severe pain. We observed overlapping expression of these Na_V channels with $K_V2.1$ in small DRG neurons (Fig. 4 and *SI Appendix*, Fig. S8), in agreement with previous analyses of unmyelinated C-fiber low-threshold mechanoreceptors, $MrgD^+$ nonpeptidergic nociceptors, and $CGRP^+$ peptidergic nociceptors (16). Na_V channel activation mediates the positive feedback mechanisms necessary to initiate an AP, and therefore changes in the availability or distribution of these channels can have a profound effect on cell excitation. AP-firing thresholds are primarily determined by Na^+ current density and the voltage dependence of activation and inactivation but are also fine-tuned by other neuronal conductances, in particular by delayed rectifier K_V channels.

The TTX-R conductance in DRG neurons is enhanced through the action of sPm1a on the voltage dependence of $Na_V1.8$ activation and inactivation, as well as its current amplitude and kinetics. In parallel, sPm1a induces a depolarizing shift in the voltage dependence of activation of the most abundant low-threshold TTX-S channel in nociceptors, $Na_V1.7$, which results in an apparent loss of current availability at hyperpolarized potentials. Substantially delayed TTX-S Na_V channel inactivation kinetics at depolarized potentials is also observed. Inactivation of the TTX-R Na^+ current is known to limit the duration of small DRG neuron firing in response to maintained stimuli, hence inactivation of $Na_V1.8$ is believed to underlie adaptation in capsaicin-sensitive small DRG neurons (33), whereas inhibition of inactivation results in sensitization to painful stimuli. Patients suffering from small fiber neuropathies carry gain-of-function mutations in $Na_V1.8$ that lower the threshold for channel activation, accelerate recovery from inactivation, impair inactivation (34), and increase resurgent currents (35). In these patients, DRG neuronal hyperexcitability is characterized by lower AP generation thresholds, increased firing rates in response to suprathreshold stimulation, and spontaneous firing, thus providing a pathophysiological basis for the reported allodynia and hyperalgesia. This neurophysiological behavior is in agreement with the observed actions of sPm1a on endogenous and recombinant $Na_V1.8$ currents, small DRG neuron sensitization, and pain behavior observed in mice.

Together with modification of $Na_V1.8$, the multimodal effects of sPm1a on DRG neuron TTX-S Na_V isoforms ($Na_V1.7$, $Na_V1.1$, and $Na_V1.6$) can perhaps contribute to the increased excitability of DRG neurons. For example, the delay in inactivation caused by sPm1a mimics gain-of-function mutations of $Na_V1.7$ that lead to increased excitability and spontaneous activity in nociceptive neurons in congenital chronic pain patients (36). Nevertheless, in any given nociceptor, the relative contribution of particular TTX-S isoforms and the extent to which their conductance and inactivation kinetics are modulated by sPm1a hinder accurate prediction.

The three main Na_V isoforms expressed in nociceptive neurons are TTX-R $Na_V1.8$ and $Na_V1.9$ and TTX-S $Na_V1.7$ (36). The major Na^+ current during an AP in small DRG somata is mediated by TTX-R $Na_V1.8$ and $Na_V1.9$ channels (37). The pulse protocol used in this study to assess small DRG neuron TTX-R favored activation of $Na_V1.8$ channels. Implementation of an alternative pulse protocol to enhance the observation of $Na_V1.9$-mediated currents showed strong potentiation of $Na_V1.8$-like currents in the presence of sPm1a but little to no $Na_V1.9$-like inward Na^+ currents in DRG neurons. Whether sPm1a also interacts with $Na_V1.9$ and how it would affect neuronal excitability and contribute to the observed in vivo nocifensive behavior in mice remains an open question. The absence of $Na_V1.9$-mediated currents in the population of mouse DRG neurons analyzed here, their small cell size, and abundance of $Na_V1.8$-mediated currents suggests a population of C-fiber nociceptors (38). Notably, the suppression of sPm1a-enhanced firing by A803467 suggests that the increase in AP firing and sensitization are largely driven by enhancement of $Na_V1.8$-mediated Na^+ currents in nociceptive DRG neurons.

The wide AP waveforms associated with pain-sensing DRG neurons, such as those in $MrgD^+$ nonpeptidergic nociceptors, allow for a large contribution of slow K_V2 currents during the AP (16), while also influencing AP repolarization. In small DRG neurons, sPm1a decreased KDR and impaired repolarization consistent with the actions of other gating-modifier venom peptides, such as GxTX-1E (κ-TRTX-Pg1a) (39) and ScTx1 (κ-TRTX-Sc1a) (22). These peptides modify $K_V2.1$ gating properties by shifting its activation to more depolarized voltages (functionally decreasing conductance) and causing neuronal hyperexcitability. Taking these data together, a key role for K_V2 channels as carriers of a sizeable proportion of the K^+ current during re- and hyperpolarization phases in sensory neurons that encode multiple pain modalities is highlighted (40).

Double immunostaining of $Na_V1.8$ and $K_V2.1$ showed 100% coincidence of these channels in small mouse sensory neurons, consistent with simultaneous detection of their encoding transcripts in >90% of these neurons using single-cell qRT-PCR (41). Yet, only 30% of the recorded DRG neurons in this study displayed a depolarized membrane potential at the end of the ramp stimulus in the presence of sPm1a. Such discrepancy may be related to the specific physiological functions of heteromeric K_V channels within particular cellular contexts, as well as major gaps in their pharmacology profiling (42). A large fraction of mouse DRG neuron KDR current is carried by homotetrameric K_V2 channels, as well as their heterotetramers with electrically "silent" α-subunits K_V5, K_V6, K_V8, and K_V9 (21, 41, 43) known to underlie subtle functional differences that fine-tune excitability patterns in diverse neuronal cell types.

Arachnid venom-derived GMPs have been shown to interact with voltage-gated calcium (Ca_V), Na_V, and K_V channels (12, 23, 44–47). We have shown here that sPm1a modulates $Na_V1.1$–$Na_V1.8$ and $K_V2.1$ channels. Experiments assessing endogenous DRG neuron high voltage-activated Ca_V currents, as well as other recombinantly expressed Ca_V and K_V channels (*SI Appendix*, Table S4), failed to identify consistent modulatory effects of sPm1a. However, given the vast array of molecular players involved in neuronal excitability, other sPm1a targets may be identified in future studies.

Pain is a complex process that involves the detection of noxious stimuli in the peripheral nervous system and processing of the nociceptive input in the central nervous system (48). Spontaneous activity in nociceptors has been described for patients with painful polyneuropathy (49). Mechanically insensitive or silent nociceptors comprise ∼30% of all C-fibers in vertebrates, with activation thresholds that are typically very high and thus are thought not to contribute to acute pain signaling (50). However, inflammation and nerve injury may lower AP-firing thresholds, thereby rendering silent nociceptors active, which might be important in mechanical hyperalgesia and central sensitization (51). Increased Na^+ influx per AP via TTX-R $Na_V1.8$ is proposed to underlie the characteristically pronounced activity-dependent slowing of conduction in mechano-insensitive, "silent" nociceptors (52). The effects of sPm1a on each nociceptive neuron would rely predominantly on the relative expression of $Na_V1.8$ and the abundance of (sensitive) delayed rectifier K channels, but also on other targets such as TTX-S Na_V channels, including $Na_V1.7$. High levels of $Na_V1.8$ expression have been reported in mechano-insensitive $CHRNA3^+$ murine nociceptors and in functionally silent porcine nociceptors (53). Unsilencing by exposure to δ/κ-TRTX-Pm1a/sPm1a upon envenomation would recruit this population of C-fibers to contribute to hyperalgesia. We propose that the lowered AP threshold and

decreased repolarization in small DRG neurons observed in the presence of sPm1a enhance neuronal excitability and is likely a key contributor to the hyperalgesic symptoms reported after *P. muticus* envenomations.

Pain caused by bites from Australian funnel-web spiders (genera *Atrax*, *Hadronyche*, and *Illawarra*) and Brazilian armed spiders (genus *Phoneutria*) is due, at least in part, to enhancement of neuronal Na_V channel activity by δ-hexatoxins and δ-phonetoxins, respectively (4, 54). Treatments for envenomation by these spiders typically involve antivenom (where available), muscle relaxants, narcotics, analgesics, and intravenous calcium (54). We showed that coadministration of A803467 (inhibiting $Na_V1.8$), or TTX (blocking $Na_V1.1$-$Na_V1.4$, $Na_V1.6$, and $Na_V1.7$), reduces sPm1a-evoked nocifensive behavior in mice, while inhibition of $Na_V1.8$ reversed sPm1a-induced hyperexcitability of DRG neurons. Hence, our results are consistent with the use of currently approved and widely available local anesthetics to relieve pain elicited by *P. muticus* envenomations.

Landmark structure–function studies have shed light on the molecular mechanism of actions of prototypical gating-modifier spider-venom peptides (55, 56). Amphipathic tarantula toxins partially partition into the membrane and interact with extracellular protein–lipid interfaces of voltage-sensor domains binding to the paddle motif (S3b helices, S3–S4 linkers, and S4 helices), and hence are also called voltage-sensor toxins (12, 46, 55–58). Pm1a's sequence, structure, and functional modification of Na_V and K_V channel gating are consistent with the action of voltage-sensor toxins. Future research aimed at uncovering the molecular details of the interaction between Pm1a and the channel targets identified herein is warranted as it may contribute important insights into the molecular mechanism of action of GMPs.

In summary, we show here that a single venom peptide can modulate three major determinants of neuronal excitability. Target promiscuity, defined as the ability to modulate the function of more than one type of receptor, is a common feature of spider toxins (23, 59). Many gating-modifier toxins are highly promiscuous and target a wide range of ion channels and receptors (23, 59). For example, Protoxin-I (β/ω-TRTX-Tp1a) from venom of the tarantula *Thrixopelma pruriens* targets a wide range of Na_V channels, $Ca_V3.1$, and TRPA1 (transient receptor potential ankyrin 1) (60). Hm1a was originally identified as a K_V channel inhibitor (61) but later recognized to elicit robust pain behaviors in mice and hypersensitivity to mechanical stimuli via potent enhancement of $Na_V1.1$ mediated currents in colonic afferents (7). Hence, Hm1a is another example of a toxin with cross-target promiscuity, ultimately resulting in the generation of pain such as we describe here for Pm1a. Recognition of common structures in different receptors has been proposed to contribute to target promiscuity (46, 56, 57, 62). Trading selectivity for functionality through the deployment of a single algogenic peptide-like δ/κ-TRTX-Pm1a to simultaneously modulate multiple receptors involved in AP generation in sensory neurons is an economic and effective tactic to evoke pain in predators as a defense strategy. Targeting a physiological function (excitability) rather than a specific molecular target (i.e., membrane protein) may represent an evolutionary adaptation of pain-producing defensive venoms. By extension, depressing neuronal excitability by targeting complementary players with "multimodal analgesics" may provide novel therapeutic alternatives for the treatment of chronic pain.

Materials and Methods

Animal experiments were conducted in accordance with the Australian National Health and Medical Research Council *Code for the Care and Use of Animals for Scientific Purposes* (63) and were approved by the local University of Queensland Animal Ethics Committee. Details of the *P. muticus* venom biochemical and bioinformatics analysis, δ/κ-TRTX-Pm1a purification, sPm1a synthesis, NMR spectroscopy, in vivo and in vitro functional characterization of sPm1a, and all materials used in this study are listed in detail in *SI Appendix, Materials and Methods*.

Data Availability. Atomic coordinates for the structure of sPm1a have been deposited in the Protein Data Bank (ID code 7JPM) (64). The chemical shifts of sPm1a were deposited in the BioMagResBank (accession code 30785) (65). Source code is deposited in Zenodo: https://doi.org/10.5281/zenodo.5009443 (29). All other study data are included in the article and/or *SI Appendix*.

ACKNOWLEDGMENTS. We thank Dr. Andrew Walker (University of Queensland) for identifying the origins of Pm1a; Dr. Mahsa Sadeghi and Ms. Anuja R. Bony for assistance with dorsal root ganglion isolation; Dr. Alejandra Rangel-Rincones for immunofluorescence and confocal microscopy assistance; Dr. Alexander Harper (University of Dundee) for insightful discussions and comments on the manuscript; L. Grum-Pau and S. D. Gatica for continuous support; Prof. Jamie Seymour and Ms. Vanessa Neale (James Cook University) for providing research materials; and Deutsche Arachnologische Gesellschaft members, especially Ingo Wendt, Michelle Luescher, Timm Adam, Frank and Claudia Schneider, Yvonne Kindl, and Hans Werner Auer for providing specimens of *P. muticus*. We acknowledge financial support from Australian National Health & Medical Research Council Program Grant APP1072113 (to P.F.A., D.J.A., and G.F.K.), Principal Research Fellowship APP1136889 (to G.F.K.), and Project Grants APP1067940 and APP1162597 (to L.D.R.); Australian Research Council Discovery Early Career Researcher Award Fellowship DE160101142 (to E.A.B.U); Centre of Excellence Grant CE200100012 (to G.F.K.); Research Council of Norway FRIPRO-YRT Fellowship 287462 (to E.A.B.U.); and Rebecca Cooper Foundation for Medical Research Grant PG2019396 (to J.R.M.). A.M. was supported by an Australian Government Research Training Program Scholarship.

1. E. Diego-García, S. Peigneur, E. Waelkens, S. Debaveye, J. Tytgat, Venom components from *Citharischius crawshayi* spider (family Theraphosidae): Exploring transcriptome, venomics, and function. *Cell. Mol. Life Sci.* **67**, 2799–2813 (2010).
2. J. K. Klint *et al.*, Isolation, synthesis and characterization of ω-TRTX-Cc1a, a novel tarantula venom peptide that selectively targets L-type Cav channels. *Biochem. Pharmacol.* **89**, 276–286 (2014).
3. T. J. Hauke, V. Herzig, Love bites—Do venomous arachnids make safe pets? *Toxicon* **190**, 65–72 (2021).
4. S. Diochot, "Pain-modulating peptides in spider venoms: Good and evil" in *Spider Venoms*, P. Gopalakrishnakone, G. A. Corzo, M. E. de Lima, E. Diego-García, Eds. (Springer Netherlands, Dordrecht, 2016), pp. 121–154.
5. D. R. Nelsen, W. Kelln, W. K. Hayes, Poke but don't pinch: Risk assessment and venom metering in the western black widow spider, *Latrodectus hesperus. Anim. Behav.* **89**, 107–114 (2014).
6. V. Herzig *et al.*, Australian funnel-web spiders evolved human-lethal δ-hexatoxins for defense against vertebrate predators. *Proc. Natl. Acad. Sci. U.S.A.* **117**, 24920–24928 (2020).
7. J. D. Osteen *et al.*, Selective spider toxins reveal a role for the Nav1.1 channel in mechanical pain. *Nature* **534**, 494–499 (2016).
8. Y. Jiang *et al.*, Pharmacological inhibition of the voltage-gated sodium channel Nav1.7 alleviates chronic visceral pain in a rodent model of irritable bowel syndrome. *ACS Pharmacol. Transl. Sci.* **4**, 1362–1378 (2021).
9. N. Ahmed, M. Pinkham, D. A. Warrell, Symptom in search of a toxin: Muscle spasms following bites by Old World tarantula spiders (*Lampropelma nigerrimum*, *Pterinochilus murinus*, *Poecilotheria regalis*) with review. *QJM* **102**, 851–857 (2009).
10. M. Mobli, G. F. King, NMR methods for determining disulfide-bond connectivities. *Toxicon* **56**, 849–854 (2010).
11. Y. Dongol, F. C. Cardoso, R. J. Lewis, Spider knottin pharmacology at voltage-gated sodium channels and their potential to modulate pain pathways. *Toxins (Basel)* **11**, 626 (2019).
12. L. R. Phillips *et al.*, Voltage-sensor activation with a tarantula toxin as cargo. *Nature* **436**, 857–860 (2005).
13. S. Lee *et al.*, Solution structure of GxTX-1E, a high-affinity tarantula toxin interacting with voltage sensors in Kv2.1 potassium channels. *Biochemistry* **49**, 5134–5142 (2010).
14. M. F. Jarvis *et al.*, A-803467, a potent and selective Nav1.8 sodium channel blocker, attenuates neuropathic and inflammatory pain in the rat. *Proc. Natl. Acad. Sci. U.S.A.* **104**, 8520–8525 (2007).
15. A. E. Dubin, A. Patapoutian, Nociceptors: The sensors of the pain pathway. *J. Clin. Invest.* **120**, 3760–3772 (2010).
16. Y. Zheng *et al.*, Deep sequencing of somatosensory neurons reveals molecular determinants of intrinsic physiological properties. *Neuron* **103**, 598–616.e7 (2019).
17. M. S. Gold, G. F. Gebhart, Nociceptor sensitization in pain pathogenesis. *Nat. Med.* **16**, 1248–1257 (2010).

PHARMACOLOGY

18. A. N. Akopian, L. Sivilotti, J. N. Wood, A tetrodotoxin-resistant voltage-gated sodium channel expressed by sensory neurons. *Nature* **379**, 257–262 (1996).
19. M. Renganathan, T. R. Cummins, S. G. Waxman, Contribution of Na(v)1.8 sodium channels to action potential electrogenesis in DRG neurons. *J. Neurophysiol.* **86**, 629–640 (2001).
20. J. Tigerholm *et al.*, Modeling activity-dependent changes of axonal spike conduction in primary afferent C-nociceptors. *J. Neurophysiol.* **111**, 1721–1735 (2014).
21. E. Bocksteins *et al.*, Kv2.1 and silent Kv subunits underlie the delayed rectifier K^+ current in cultured small mouse DRG neurons. *Am. J. Physiol. Cell Physiol.* **296**, C1271–C1278 (2009).
22. C. Tsantoulas *et al.*, Kv2 dysfunction after peripheral axotomy enhances sensory neuron responsiveness to sustained input. *Exp. Neurol.* **251**, 115–126 (2014).
23. F. Bosmans, K. J. Swartz, Targeting voltage sensors in sodium channels with spider toxins. *Trends Pharmacol. Sci.* **31**, 175–182 (2010).
24. S. D. Dib-Hajj *et al.*, Gain-of-function mutation in Nav1.7 in familial erythromelalgia induces bursting of sensory neurons. *Brain* **128**, 1847–1854 (2005).
25. A. M. Rush *et al.*, A single sodium channel mutation produces hyper- or hypoexcitability in different types of neurons. *Proc. Natl. Acad. Sci. U.S.A.* **103**, 8245–8250 (2006).
26. S. D. Dib-Hajj, P. Geha, S. G. Waxman, Sodium channels in pain disorders: Pathophysiology and prospects for treatment. *Pain* **158** (suppl. 1), S97–S107 (2017).
27. P. Verma *et al.*, Examining sodium and potassium channel conductances involved in hyperexcitability of chemotherapy-induced peripheral neuropathy: A mathematical and cell culture-based study. *Front. Comput. Neurosci.* **14**, 564980 (2020).
28. S. Heitmann, M. Breakspear, *Handbook for the Brain Dynamics Toolbox*: Version 2020 (bdtoolbox.org, 5th ed., 2020).
29. S. Heitmann, J. R. McArthur, A. P. Hill, Control and Spm1a modified Nav1.8 and TTX-s sodium channel models. *Zenodo*. https://dx.doi.org/10.5281/zenodo.5009443. Deposited 2021.
30. D. Mandge, R. Manchanda, A biophysically detailed computational model of urinary bladder small DRG neuron soma. *PLoS Comput. Biol.* **14**, e1006293 (2018).
31. J. S. Choi, S. G. Waxman, Physiological interactions between Na(v)1.7 and Na(v)1.8 sodium channels: A computer simulation study. *J. Neurophysiol.* **106**, 3173–3184 (2011).
32. S. Jami, A. Erickson, S. M. Brierley, I. Vetter, Pain-causing venom peptides: Insights into sensory neuron pharmacology. *Toxins (Basel)* **10**, 15 (2017).
33. N. T. Blair, B. P. Bean, Role of tetrodotoxin-resistant Na^+ current slow inactivation in adaptation of action potential firing in small-diameter dorsal root ganglion neurons. *J. Neurosci.* **23**, 10338–10350 (2003).
34. C. Han, J. Huang, S. G. Waxman, Sodium channel Nav1.8: Emerging links to human disease. *Neurology* **86**, 473–483 (2016).
35. Y. Xiao *et al.*, Increased resurgent sodium currents in Nav1.8 contribute to nociceptive sensory neuron hyperexcitability associated with peripheral neuropathies. *J. Neurosci.* **39**, 1539–1550 (2019).
36. G. Goodwin, S. B. McMahon, The physiological function of different voltage-gated sodium channels in pain. *Nat. Rev. Neurosci.* **22**, 263–274 (2021).
37. N. T. Blair, B. P. Bean, Roles of tetrodotoxin (TTX)-sensitive Na^+ current, TTX-resistant Na^+ current, and Ca^{2+} current in the action potentials of nociceptive sensory neurons. *J. Neurosci.* **22**, 10277–10290 (2002).
38. D. E. Duzhyy, V. Y. Viatchenko-Karpinski, E. V. Khomula, N. V. Voitenko, P. V. Belan, Upregulation of T-type Ca^{2+} channels in long-term diabetes determines increased excitability of a specific type of capsaicin-insensitive DRG neurons. *Mol. Pain* **11**, 29 (2015).
39. T. Kimm, Z. M. Khaliq, B. P. Bean, Differential regulation of action potential shape and burst-frequency firing by BK and Kv2 channels in substantia nigra dopaminergic neurons. *J. Neurosci.* **35**, 16404–16417 (2015).
40. C. Tsantoulas, S. B. McMahon, Opening paths to novel analgesics: The role of potassium channels in chronic pain. *Trends Neurosci.* **37**, 146–158 (2014).
41. M. C. Lee *et al.*, Human labor pain is influenced by the voltage-gated potassium channel Kv6.4 subunit. *Cell Rep.* **32**, 107941 (2020).
42. M. J. Giacobassi *et al.*, An integrative approach to the facile functional classification of dorsal root ganglion neuronal subclasses. *Proc. Natl. Acad. Sci. U.S.A.* **117**, 5494–5501 (2020).
43. G. Regnier, E. Bocksteins, G. Van de Vijver, D. J. Snyders, P. P. van Bogaert, The contribution of Kv2.2-mediated currents decreases during the postnatal development of mouse dorsal root ganglion neurons. *Physiol. Rep.* **4**, e12731 (2016).
44. A. Salari, B. S. Vega, L. S. Milescu, M. Milescu, Molecular interactions between tarantula toxins and low-voltage-activated calcium channels. *Sci. Rep.* **6**, 23894 (2016).
45. J. R. McArthur, N. R. Munasinghe, R. K. Finol-Urdaneta, D. J. Adams, M. J. Christie, Spider venom peptide Pn3a inhibition of primary afferent high voltage-activated calcium channels. *Front. Pharmacol.* **11**, 633679 (2021).
46. Y. Li-Smerin, K. J. Swartz, Gating modifier toxins reveal a conserved structural motif in voltage-gated Ca^{2+} and K^+ channels. *Proc. Natl. Acad. Sci. U.S.A.* **95**, 8585–8589 (1998).
47. F. C. Cardoso, Multi-targeting sodium and calcium channels using venom peptides for the treatment of complex ion channels-related diseases. *Biochem. Pharmacol.* **181**, 114107 (2020).
48. M. A. Mis *et al.*, Resilience to pain: A peripheral component identified using induced pluripotent stem cells and dynamic clamp. *J. Neurosci.* **39**, 382–392 (2019).
49. I. P. Kleggetveit *et al.*, High spontaneous activity of C-nociceptors in painful polyneuropathy. *Pain* **153**, 2040–2047 (2012).
50. R. Schmidt, M. Schmelz, H. E. Torebjörk, H. O. Handwerker, Mechano-insensitive nociceptors encode pain evoked by tonic pressure to human skin. *Neuroscience* **98**, 793–800 (2000).
51. J. Tigerholm *et al.*, C-fiber recovery cycle supernormality depends on ion concentration and ion channel permeability. *Biophys. J.* **108**, 1057–1071 (2015).
52. M. E. Petersson *et al.*, Differential axonal conduction patterns of mechano-sensitive and mechano-insensitive nociceptors—A combined experimental and modelling study. *PLoS One* **9**, e103556 (2014).
53. R. Jonas *et al.*, TTX-resistant sodium channels functionally separate silent from polymodal C-nociceptors. *Front. Cell. Neurosci.* **14**, 13 (2020).
54. G. K. Isbister, H. W. Fan, Spider bite. *Lancet* **378**, 2039–2047 (2011).
55. M. Mihailescu *et al.*, Structural interactions of a voltage sensor toxin with lipid membranes. *Proc. Natl. Acad. Sci. U.S.A.* **111**, E5463–E5470 (2014).
56. M. Milescu *et al.*, Interactions between lipids and voltage sensor paddles detected with tarantula toxins. *Nat. Struct. Mol. Biol.* **16**, 1080–1085 (2009).
57. J. R. Winterfield, K. J. Swartz, A hot spot for the interaction of gating modifier toxins with voltage-dependent ion channels. *J. Gen. Physiol.* **116**, 637–644 (2000).
58. K. M. Van Theemsche, D. V. Van de Sande, D. J. Snyders, A. J. Labro, Hydrophobic drug/toxin binding sites in voltage-dependent K^+ and Na^+ channels. *Front. Pharmacol.* **11**, 735 (2020).
59. E. Redaelli *et al.*, Target promiscuity and heterogeneous effects of tarantula venom peptides affecting Na^+ and K^+ ion channels. *J. Biol. Chem.* **285**, 4130–4142 (2010).
60. J. Gui *et al.*, A tarantula-venom peptide antagonizes the TRPA1 nociceptor ion channel by binding to the S1-S4 gating domain. *Curr. Biol.* **24**, 473–483 (2014).
61. P. Escoubas, S. Diochot, M. L. Célérier, T. Nakajima, M. Lazdunski, Novel tarantula toxins for subtypes of voltage-dependent potassium channels in the Kv2 and Kv4 subfamilies. *Mol. Pharmacol.* **62**, 48–57 (2002).
62. Z. Liao *et al.*, Solution structure and functional characterization of Jingzhaotoxin-XI: A novel gating modifier of both potassium and sodium channels. *Biochemistry* **45**, 15591–15600 (2006).
63. Australian National Health and Medical Research Council, *Australian Code for the Care and Use of Animals for Scientific Purposes* (Australian Research Council, 8th Ed, 2013).
64. Y. K.-Y. Chin, R. Ziegman, P. F. Alewood, The solution structure of omega-theraphotoxin-Pm1b isolated from King Baboon spider. RCSB Protein Data Bank. https://www.rcsb.org/structure/7JPM. Deposited 9 August 2020.
65. Y. Chin, R. Ziegman, P. Alewood, The solution structure of omega-theraphotoxin-Pm1b isolated from King Baboon spider. Biological Magnetic Resonance Data Bank. https://bmrb.io/data_library/summary/index.php?bmrbId=30785. Deposited 9 August 2020.